

HUBBLE/COS OBSERVATIONS OF THE LY α FOREST TOWARD THE BLLAC OBJECT 1ES1553+113*

CHARLES W. DANFORTH, BRIAN A. KEENEY, JOHN T. STOCKE, J. MICHAEL SHULL, & YANGSEN YAO
CASA, Department of Astrophysical & Planetary Sciences, University of Colorado, 389-UCB, Boulder, CO 80309;
danforth@casa.colorado.edu
ApJ submitted May 11, 2010

ABSTRACT

We present new moderate-resolution, far-ultraviolet spectra from the *Hubble Space Telescope*/Cosmic Origins Spectrograph (HST/COS) of the BL Lac object 1ES1553+113 covering the wavelength range $1135 \text{ \AA} < \lambda < 1795 \text{ \AA}$. The data show a smooth continuum with a wealth of narrow ($b < 100 \text{ km s}^{-1}$) absorption features arising in the interstellar medium (ISM) and intergalactic medium (IGM). These features include 41 Ly α absorbers at $0 < z_{\text{abs}} < 0.43$, fourteen of which are detected in multiple Lyman lines and six of which show absorption in one or more metal lines. We analyze a metal-rich triplet ($\Delta cz \sim 1000 \text{ km s}^{-1}$) of Ly α absorbers at $z_{\text{abs}} \approx 0.188$ in which O VI, N V, and C III absorption is detected. Silicon ions (Si III, Si IV) are not detected to fairly strong upper limits, and we use the measured Si III/C III upper limit to derive an abundance limit $(\text{C/Si}) \geq 4(\text{C/Si})_{\odot}$ for the strongest component of the absorber complex. Galaxy redshift surveys show a number of massive galaxies at approximately the same redshift as this absorption complex, suggesting that it arises in a large-scale galaxy filament. As one of the brightest extragalactic X-ray and γ -ray sources, 1ES1553+113 is of great interest to the high-energy astrophysics community. With no intrinsic emission or absorption features, 1ES1553+113 has no direct redshift determination. We use intervening Ly α absorbers to place a direct limit on the redshift: $z_{\text{em}} > 0.395$ based on a confirmed Ly α +O VI absorber and $z_{\text{em}} > 0.433$ based on a single-line detection of Ly α . The current COS data are only sensitive to Ly α absorbers at $z < 0.47$, but we present statistical arguments that $z_{\text{em}} \lesssim 0.58$ (at a 1σ confidence limit) based on the non-detection of any Ly β absorbers at $z > 0.4$.

Subject headings: BL Lacertae objects: individual: 1ES1553+113, galaxies: active, intergalactic medium, quasars: absorption lines, ultraviolet: general

1. INTRODUCTION

The current interpretation of BL Lac objects (Ghisellini, Maraschi, & Treves 1985) is that they are active galactic nuclei (AGN) with a strongly relativistic jet pointed toward our line of sight. As such, any line emission or accretion disk features seen in most other types of AGN could be masked by the bright jet if present in BL Lac objects. Their spectra usually show a featureless power-law continuum extending from radio to X-ray wavelengths. This spectral characteristic makes BL Lac objects ideal for observing intervening absorption features arising in the interstellar medium (ISM) and intergalactic medium (IGM). Since their continuum is easily defined, they make excellent targets for studying weak metal-line systems and low-contrast, highly thermally broadened H I absorbers (e.g., Richter et al. 2004; Lehner et al. 2007; Danforth, Stocke & Shull 2010).

The BL Lac object 1ES1553+113 shows the characteristic featureless power-law spectrum and is one of the brightest known sources of extragalactic high-energy radiation from X-rays up to VHE (TeV) photons (Costamante & Ghisellini 2002). However, the featureless spectrum makes it difficult to determine the redshift of the object and hence its luminosity. Indirect methods have given a wide range of limits for the redshift of

1ES1553+113; the nondetection of a host galaxy gave limits from $z_{\text{em}} > 0.09$ to $z_{\text{em}} > 0.78$ (Hutchings & Neff 1992; Scarpa et al. 2000; Urry et al. 2000; Carangelo et al. 2003; Sbaruffatti et al. 2006; Treves, Falomo, & Uslenghi 2007). The shape of the γ -ray spectrum observed by the *Fermi Observatory* and ground-based VHE detectors (HESS, MAGIC) constrains the redshift to values from $z_{\text{em}} < 0.4$ to $z_{\text{em}} < 0.8$ (Aharonian et al. 2006; Albert et al. 2007; Mazin & Goebel 2007; Abdo et al. 2010) based on assumptions about the intrinsic spectral energy distribution (SED) and pair-production interactions with the cosmic infrared background. The only direct redshift determination ($z_{\text{em}} = 0.36$; Miller & Green 1983) was based on a spurious feature in low-resolution UV spectra from the *International Ultraviolet Explorer* (IUE). The detection was later retracted (Falomo & Treves 1990), but the erroneous redshift value lives on.

1ES1553+113 is of interest as a bright background continuum source for detecting intergalactic absorption along the sight line. Bright X-ray sources are especially valuable for potentially detecting the long-predicted O VII and O VIII tracers (Bregman 2007) of intergalactic gas at $T = 10^6 - 10^7 \text{ K}$. Even for a bright X-ray source, the required integration times would be very long. However, a sufficiently long IGM pathlength provided by a bright high- z target would make the required observing time investment more attractive.

In this paper, we present the first medium-resolution far-UV spectroscopic observations of 1ES1553+113 including *Hubble Space Telescope*/Cosmic Origins Spectrograph (HST/COS Green et al. 2010; Osterman et al.

*BASED ON OBSERVATIONS MADE WITH THE NASA/ESA HUBBLE SPACE TELESCOPE, OBTAINED FROM THE DATA ARCHIVE AT THE SPACE TELESCOPE SCIENCE INSTITUTE. STSCI IS OPERATED BY THE ASSOCIATION OF UNIVERSITIES FOR RESEARCH IN ASTRONOMY, INC. UNDER NASA CONTRACT NAS 5-26555.

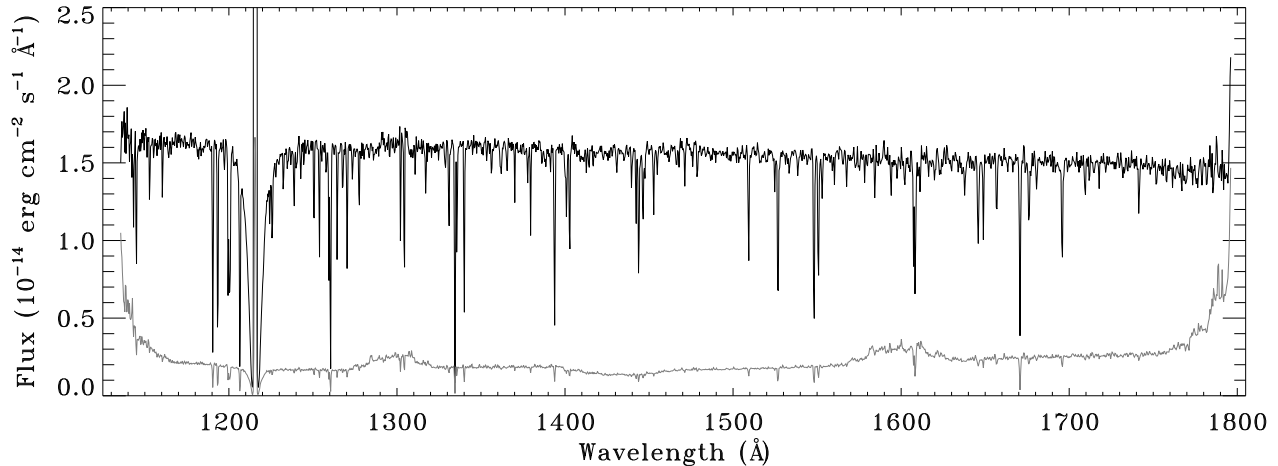


FIG. 1.— Overview of the COS spectrum of 1ES 1553+113. The full COS/G130M+G160M dataset is shown, smoothed by 35 pixels (~ 5 resolution elements). Error is shown in gray.

2010) observations ($\lambda = 1135 - 1795 \text{ \AA}$) as well as archival data at $905 - 1187 \text{ \AA}$ from the *Far Ultraviolet Spectroscopic Explorer* (*FUSE*; Moos et al. 2000; Sahnou et al. 2000). We confirm the featureless power-law nature of the spectrum over this wavelength range. Absorption is seen in 42 intervening systems including 41 Ly α absorbers and six metal-line systems. The frequency of IGM absorbers is consistent with larger surveys using *FUSE* and HST/STIS data (Danforth & Shull 2005, 2008; hereafter DS08), and the systems are spread across the entire redshift range covered by the combined COS/*FUSE* dataset ($z \lesssim 0.47$).

The observations and data reduction techniques are discussed in §2, and we present a preliminary catalog of absorption lines in §3. Our conclusions are presented in §4.

2. OBSERVATIONS AND DATA ANALYSIS

Far-UV observations of 1ES 1553+113 were carried out 2009 September 22 by HST/COS as part of the COS Guaranteed Time Observations (PID 11528, PI Green). Five exposures were made in each of the G130M ($1135 < \lambda < 1480 \text{ \AA}$) and G160M ($1400 < \lambda < 1795 \text{ \AA}$) medium-resolution gratings ($R \approx 18,000$) totalling 3.1 and 3.8 ksec, respectively. Four central wavelength settings at each grating dithered known instrumental features along the spectrum and provided continuous spectral coverage over $1135 < \lambda < 1795 \text{ \AA}$ (see Green et al. 2010; Osterman et al. 2010). After retrieval from the archive, all ten exposures were reduced locally using CALCOS v2.11F.

Flat-fielding, alignment, and coaddition of the processed exposures were carried out using IDL routines developed by the COS GTO team specifically for COS FUV data¹. First, the data were corrected for the most egregious instrumental features. While attempts at a true “flat-fielding” of COS data show promise, the technique is not yet robust enough to improve data of moderate S/N. However, we are able to correct the narrow $\sim 15\%$ -opaque features arising from ion repeller grid wires in

the detector. A one-dimensional map of grid-wire opacity for each detector was shifted from detector coordinates into wavelength space and divided from the flux and error vectors. Exposure time in the location of grid wires was decreased to $\sim 70\%$, giving these pixels less weight in the final coaddition. We also modify the error and local exposure time at the edges of the detector segments to de-weight flux contributions from these regions. With four different central wavelength settings per grating, any residual instrumental artifacts from grid-wire shadows and detector segment boundaries should have negligible effect on the final spectrum.

The exposures are aligned with each other and interpolated onto a common wavelength scale. One exposure in each grating/detector was picked as a wavelength reference, and the remaining exposures were cross-correlated with it. The wavelength region of cross-correlation for each case was picked to include a strong ISM absorption feature, and shifts were typically on the order of a resolution element ($\sim 0.07 \text{ \AA}$) or less. The COS wavelength solution has not yet been rigorously characterized, and we see a systematic shift between strong ISM lines and their expected LSR velocities. The shift is approximately constant across the COS wavelength range, so we apply a uniform $+0.17 \text{ \AA}$ shift to the wavelength vectors ($\sim 40 \text{ km s}^{-1}$ at $\sim 1300 \text{ \AA}$) to bring ISM line centroids to the expected $v_{\text{LSR}} \approx 0$ seen in many ISM absorbers.

Next, the aligned exposures were interpolated onto a uniform wavelength grid and coadded. The flux at each position was taken to be the exposure-weighted mean of flux in each exposure. Since exposure time was reduced in certain wavelength locations, as noted above, pixels near detector edges and where grid-wire shadows were removed received less weight than those in less suspect locations. The combined data show $S/N \sim 20$ per 7-pixel ($\sim 0.07 \text{ \AA}$) resolution element and are sufficient to detect narrow absorption features down to $W_\lambda \approx 15 \text{ m\AA}$ at 4σ significance. Figure 1 shows the entire combined COS/G130M and COS/G160M spectra. Figure 2 shows a more detailed view of the spectrum with prominent lines marked.

In addition to the COS data, we utilize 45 ksec of *Far*

¹ See <http://casa.colorado.edu/~danforth/costools.html> for our coaddition and flat-fielding algorithm and additional discussion.

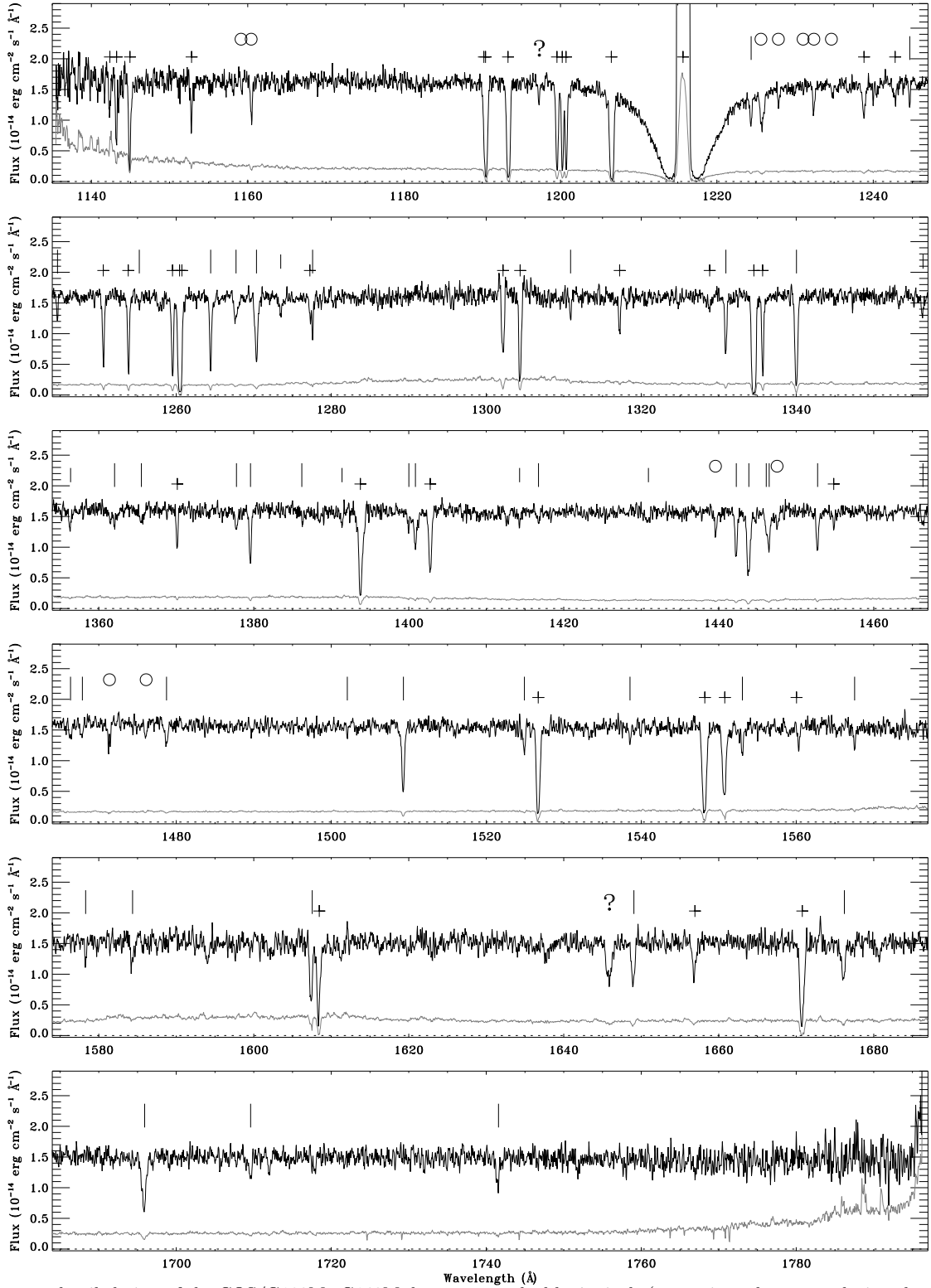


FIG. 2.— A more detailed view of the COS/G130M+G160M dataset smoothed by 7 pixels (approximately one resolution element). Error is shown in gray. Prominent ISM lines are marked with plus signs. IGM Ly α absorbers are marked with large vertical ticks. Smaller ticks denote corresponding Ly β detections. IGM metal absorbers are marked with open circles. The two question marks denote the ambiguous features discussed in §3. See Table 1 for line identifications and measurements.

Ultraviolet Spectroscopic Explorer (FUSE) observations taken 2004 April as part of program E526 (PI: Savage). While *FUSE* data alone are insufficient to characterize the H I absorber systems along a sight line, far-UV coverage is invaluable for confirming Ly α lines at $z \lesssim 0.11$ via Ly β absorption. Additionally, O VI $\lambda\lambda 1032, 1038$ and C III $\lambda 977$ absorbers are found only in *FUSE* data at $z < 0.10$ and $z < 0.16$, respectively. Thirty-seven *FUSE* exposures were retrieved from the archive and processed in the usual manner (Danforth & Shull 2005). The final *FUSE* spectrum covers $\lambda = 905 - 1187 \text{ \AA}$ with $S/N \approx 7 - 10$ per $\sim 20 \text{ km s}^{-1}$ resolution element.

3. ABSORPTION LINES

An initial analysis of the spectrum reveals a wealth of far-UV absorption features (Figures 1 and 2). Many of these are clearly Galactic ISM lines typical of most sight lines to Galactic and extragalactic sources. We label the remainder as redshifted IGM absorbers. To identify these lines, we follow a procedure similar to that employed in DS08: starting from the long-wavelength end of the spectrum, we interactively mark the strongest absorption features, tentatively identifying them as Ly α . The location of the corresponding Ly β absorption is then checked, as are those of prominent metal-ion absorbers (O VI $\lambda\lambda 1032, 1038$; C IV $\lambda\lambda 1548, 1550$; Si III $\lambda 1207$; C III $\lambda 977$, etc.). This process is iterative, as we iden-

tify weaker and weaker features. If there is component structure in a line profile that can be unambiguously deconvolved into multiple absorbers, we list these systems separately. However, most systems are listed as a single absorber, even if they possess rather complex line profiles.

We note two significant absorption features at 1197.25 \AA and 1645.9 \AA with highly ambiguous identifications. The weak feature at 1197.25 \AA ($W_{\text{obs}} \approx 50 \text{ m\AA}$) cannot be Ly α , nor is it consistent with either a higher-order Lyman line or any obvious metal-ion absorber for any of the known H I systems. The most plausible identification is that of O VI $\lambda 1038$ at $z = 0.1538$ (Fig. 3). The stronger $\lambda 1032$ line of the O VI doublet is blended with Galactic Si II $\lambda 1190$. No H I absorption is seen at this redshift in Ly β , and a 4σ upper limit on the column-density can be set at $\log N_{\text{HI}} < 13.81$. Ly α absorption at this redshift is blended with the weaker line of the Galactic Si IV doublet at $\lambda 1403$. However, the Galactic Si IV lines appear in the expected 2:1 ratio, leaving little room for additional blended Ly α $z = 0.1538$ absorption. It appears possible that this is a WHIM absorber with high enough temperature and metallicity that no neutral gas is seen (see also Savage et al. 2010).

The strong absorption line at 1645.9 \AA ($W_{\text{obs}} \approx 357 \text{ m\AA}$) could be identified as Ly α at $z = 0.3539$, but the expected Ly β absorber ($W_{\text{obs}} \geq 50 \text{ m\AA}$) is not seen (Fig. 4a,b). The line is consistent with being Ly β absorption at $z = 0.6046$, and an equivalent Ly γ feature is seen at 1560.3 \AA at approximately the expected strength (Fig. 4a,c). However, the latter feature is consistent with Galactic C I absorption lines seen elsewhere in the data (Fig. 4d-f). Therefore, we tentatively identify this feature as a multi-component Ly α system at $z = 0.3539$. Two or more Ly β features of the required strengths can plausibly be hidden in the noise at the required location.

Table 1 lists measurements for all detected IGM absorption lines, grouped by redshift, and including the two ambiguous cases above. In total, we identify 42 IGM absorbers (Table 1), 41 of which are detected in at least Ly α . Corresponding higher-order Lyman line and/or metal ion absorption is seen in 15 absorbers. Seven systems show metal absorption. The observed Ly α absorber frequency per unit redshift, $dN/dz \approx 87 \pm 15$, down to a limiting equivalent width of 50 m \AA ($\sim 10^{13} \text{ cm}^{-2}$), is similar to that found for the larger DS08 sample to the same limit ($dN/dz = 95 \pm 5$). A more thorough search for broad Ly α absorbers with $b > 40 \text{ km s}^{-1}$ will be conducted, following the receipt of additional data on this source scheduled for Cycle 18. Therefore, we caution the reader that this line list may not be complete for lines with $b > 40 \text{ km s}^{-1}$.

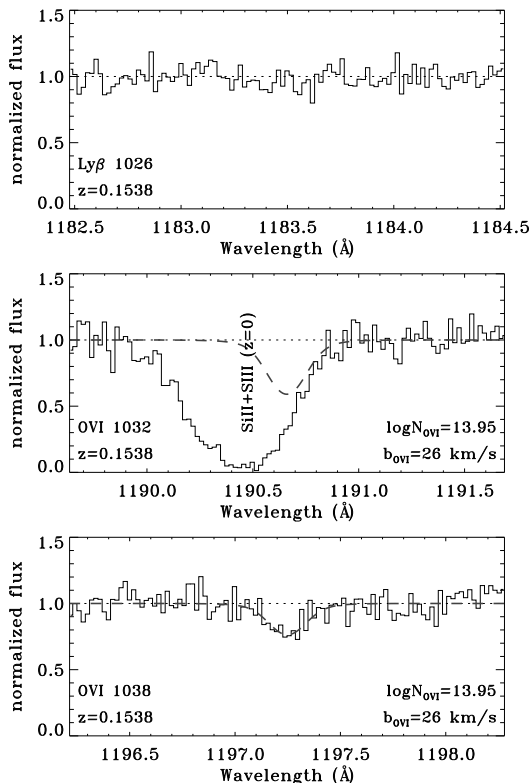


FIG. 3.— A weak absorption line at 1197.25 \AA ($W_{\lambda} = 50 \pm 9 \text{ m\AA}$) is consistent with O VI $\lambda 1038$ at $z = 0.1538$ (bottom panel). The corresponding O VI $\lambda 1032$ line is blended with Galactic Si II+S III absorption, but consistent with the measurement from the O VI $\lambda 1038$ line (middle panel). The corresponding Ly α absorber is blended with Galactic Si IV $\lambda 1403$, but no H I is seen in Ly β (top panel) to 4σ limit $\log N_{\text{HI}} < 13.81$.

4. RESULTS AND DISCUSSION

An additional six orbits of COS integration time planned for Cycle 18 should improve the S/N of the combined dataset by a factor of ~ 2 . Greatly improved S/N, as well as our evolving understanding of the COS instrumental effects, will enable us to reliably measure low-contrast absorbers such as broad Ly α systems and weak metal lines. We defer a more exhaustive analysis of the sight line until then, but note two key results here.

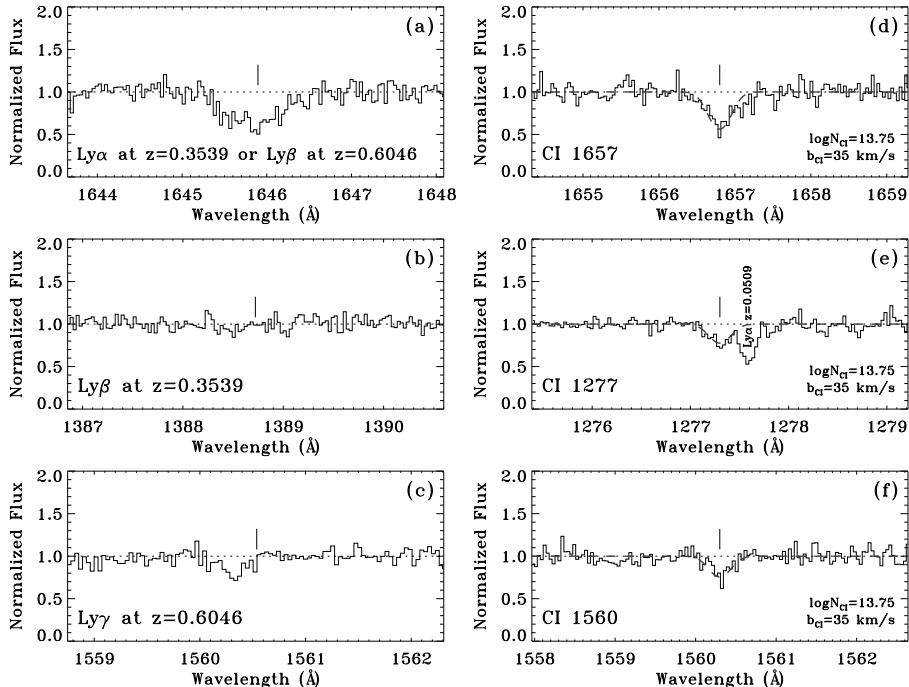


FIG. 4.— A broad feature at 1645.9 Å (panel a) is interpreted as Ly α at $z = 0.3539$. However, the expected Ly β feature (panel b) is not seen in the data. If the 1645.9 Å feature is instead interpreted as Ly β at $z = 0.6046$, a feature of approximately the correct strength is seen at 1560.3 Å, the location of the expected Ly γ at $z = 0.6046$ (panel c). However, the 1560.3 Å feature is consistent with Galactic CI absorption (dashed profile in panels d-f). We conclude that the 1645.9 Å feature is most likely a multi-component Ly α absorber at $z \approx 0.3539$, but the individual components are too weak to appear in Ly β .

4.1. Triple Absorber Complex at $z = 0.188$

The most interesting of the previously undiscovered IGM absorption systems is the triplet of metal-rich absorbers at $z = 0.18640, 0.18773, \text{ and } 0.18989$ (Figure 5). In Ly α , the strong central absorber at $z = 0.18773$ is flanked by two weaker components at $z = 0.18640$ and $z = 0.18989$, or $v = -399 \text{ km s}^{-1}$ and $v = +648 \text{ km s}^{-1}$, respectively, relative to the system at $z = 0.18773$.

The three absorption systems at $z \sim 0.188$ span $\sim 1000 \text{ km s}^{-1}$ in comoving velocity space, appropriate for a large-scale filament in the cosmic web. We searched the SDSS Data Release 7 galaxy redshift catalog (Abazajian et al. 2009) for galaxies within one degree of the 1ES1553+113 sight line and plotted them as a function of redshift (Fig. 6, top panel). While the SDSS is complete only in the brightest galaxies ($L \gtrsim 3 L^*$) at this redshift, a clear concentration appears at $z = 0.187 \pm 0.003$. None of these galaxies is closer than 24' ($\sim 4.5 \text{ Mpc}$ at $z = 0.188$) to the line of sight, so it is hard to claim a specific galaxy-absorber relationship (Figure 6, bottom panel). However, the median redshift of the galaxy sample is $z = 0.187$ and the 1σ deviation ($\sigma_z = 0.0027$) is roughly one-third of the redshift search space ($\Delta z = \pm 0.008$). This tight clustering around the absorber redshift, as well as the observed spatial distribution of the brightest galaxies, suggests that the galaxies trace a large-scale filament in the cosmic web and that the absorption in the COS observations arises in the same structure. Deeper galaxy survey work (Keeney et al., in preparation) is complete to much lower luminosity ($L \gtrsim 0.3 L^*$) and may show a closer galaxy-absorber relationship.

O VI absorption is seen in all three systems ($\log N_{\text{OVI}} = 13.4 \pm 0.3, 14.1 \pm 0.1, \text{ and } 13.5 \pm 0.1$, respectively). Strong N V absorption is seen in the central component ($\log N_{\text{NV}} = 13.7 \pm 0.1$). DS08 measure $\langle N_{\text{NV}}/N_{\text{OVI}} \rangle = 0.24^{+0.22}_{-0.12}$ in eleven O VI+N V low- z IGM absorbers, so the ratio observed at $z = 0.18773$ toward 1ES 1553+113 ($N_{\text{NV}}/N_{\text{OVI}} = 0.4$) is high but within the observed range. The DS08 sample is a biased toward higher N_{NV} values, the observed ratio suggests an elevated N/O abundance in this absorber.

C III is detected in the central and blue components ($\log N_{\text{CIII}} = 13.25^{+0.06}_{-0.04}$ and 12.64 ± 0.15 , respectively), but 4σ upper limits of $\log N_{\text{SiIII}} < 11.64$ and $\log N_{\text{SiIV}} < 12.29$ can be placed on Si-ion absorption in all three systems. Si II $\lambda 1260$ is tentatively detected at $z = 0.1877$ as a pair of weak, narrow components with a total column density $\log N_{\text{SiII}} \sim 12.1$. However, we do not detect other Si II lines, nor equivalent absorption in C II $\lambda 1334.5$ or C II $\lambda 1036.3$ ($\log N_{\text{CII}} \leq 12.82$) and other singly-ionized species.

It is likely that the gas in the central $z = 0.1877$ Ly α system is multi-phase in nature, with a warm-hot ionized medium (WHIM) component traced by O VI and N V and a cooler, photoionized component traced by H I and C III. The “multiphase ratios” for these absorbers (Danforth & Shull 2005, 2008) are $N_{\text{HI}}/N_{\text{OVI}} \sim 1.3, \sim 0.6$, and ~ 0.5 for the three main components. Typical values for absorbers with similar N_{HI} are $\sim 0.6, \sim 2.5$, and ~ 0.8 , respectively (Danforth & Shull 2005). We can use the Ly α and low-ionization metal detections and upper limits to constrain metallicity and relative abundances in the photoionized gas. In particular, C III and Si III

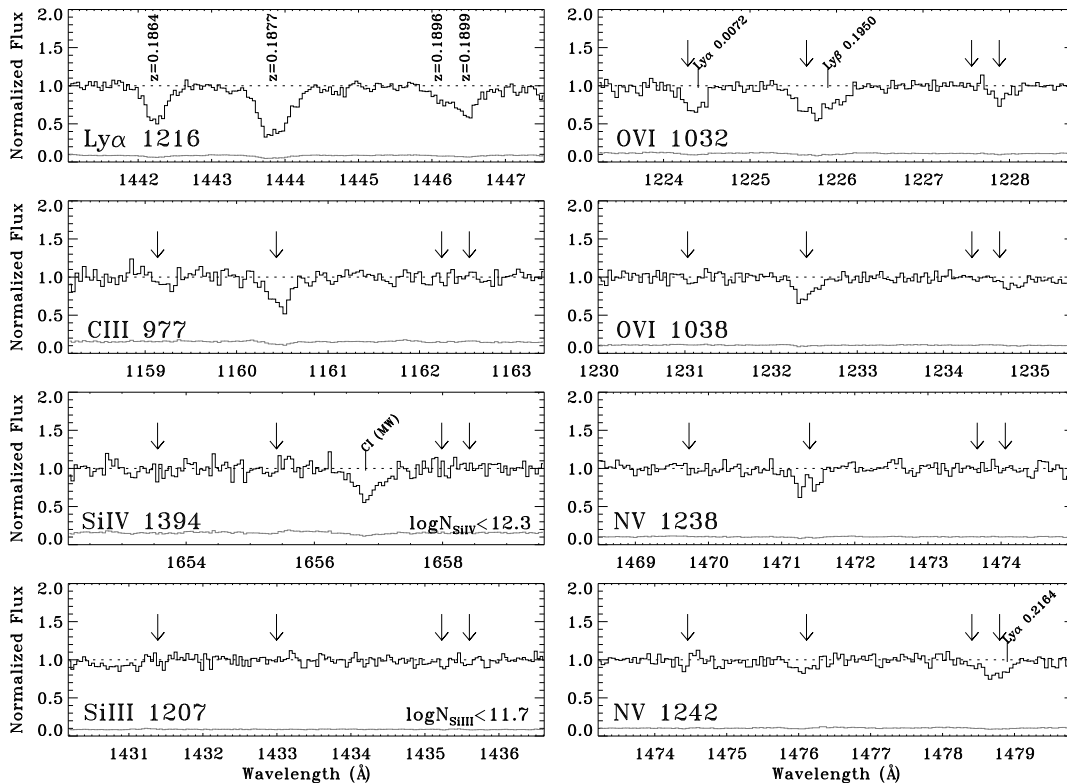


FIG. 5.— Detail of the absorption complex at $z = 0.188$. Top left panel shows three strong Ly α absorption systems at $z = 0.1864$, $z = 0.1877$, and $z = 0.1897$. The reddest of these is clearly split into two components ($z = 0.18958$ and $z = 0.18989$). The strong, central absorber also shows clear evidence of multiple structure, but is harder to deconvolve unambiguously. In subsequent panels, these components are marked by arrows. Corresponding metal absorption is detected in several of these components in C III, O VI, and NV, however there is no measurable absorption in either Si III or Si IV. Several unrelated lines appear in the profiles and are labeled with vertical ticks. Data is binned by four pixels ($\sim 50\%$ of a resolution element).

have similar ionization potentials and are often detected in the same systems. At solar abundance ratios (Asplund et al. 2009), carbon is 8.3 times more abundant than silicon, but Si III is detectable to much lower column densities than C III owing to the very strong f -value of the 1206.5 Å transition (Shull et al. 2009). Thus, the two ions are often seen together in photoionized IGM absorbers (DS08).

We measure $N_{\text{CIII}}/N_{\text{SiIII}} > 40$ in the $z = 0.1877$ absorber, an unusually high lower limit. DS08 report C III and Si III detections in 22 low- z IGM systems with a median distribution of $N_{\text{CIII}}/N_{\text{SiIII}} = 8.5^{+20.4}_{-5.5}$ (1σ). In Galactic High Velocity Clouds (Fox, Savage, & Wakker 2006; Shull et al. 2009) the ratio, $N_{\text{CIII}}/N_{\text{SiIII}}$, typically ranges from 5–20. Thus, the abnormally high ratio ~ 40 found in these IGM absorbers is well outside the usual range. Comparing our measurements with a grid of simple CLOUDY photoionization models (detailed in Danforth et al. 2006), we see that the relative column densities of C III and Si III are fairly insensitive to photoionization parameter $U \equiv n_{\gamma}/n_H$. Typical model ratios are $(N_{\text{CIII}}/N_{\text{SiIII}}) \sim 10$ in the expected range of IGM photoionization parameters ($U \sim 10^{-2}$) and are largely insensitive to assumptions about metallicity, photon continuum, and gas density.

The unusually high C III/Si III ratio suggests that the C/Si abundance in this system may have a strongly non-solar abundance pattern. If N_{SiIII} is typically $\sim 10\%$ of

N_{CIII} , as seen in other IGM observations and models, $[\text{Si}/\text{C}] > 0.6$, or greater than four times the solar value. Comparing the observed $N_{\text{CIII}}/N_{\text{HI}}$ ratio with the models, we expect $\log(N_{\text{CIII}}/N_{\text{HI}}) \lesssim -1.7$ for $Z = 0.1 Z_{\odot}$. However, the observed column density ratio is an order of magnitude higher, suggesting that (C/H) is close to solar values in this system. Without additional low-ionization species detected, we cannot determine whether carbon is overabundant or silicon is underabundant relative to the solar ratio. The C III detection at $z = 0.1864$ is factor of four weaker than in the main absorber, while the upper limit on N_{SiIII} is the same. Therefore, this system puts weak constraints on the metallicity and abundances in this absorber.

Although $(\text{C}/\text{Si}) = 8.3 \pm 1.2$ in the Sun (Asplund et al. 2009), variations in this abundance ratio can occur, depending on the youth of the stellar population and its initial mass function (IMF). Carbon is produced primarily by helium burning in intermediate-mass stars (red giants, horizontal branch), whereas silicon arises from more advanced α -process nucleosynthesis in massive stars. The usual abundance trends show enhanced (Si/C) and reduced (N/O) in low-metallicity stellar populations (McWilliam 1997; Cayrel et al. 2004). Theoretical predictions (Woosley & Weaver 1995) show that $[\alpha/\text{Fe}]$ increases with increasing progenitor mass (here, α includes O, Mg, Si, S, Ca, Ti). Thus, a low Si and O abundance compared to C and N suggests an IMF

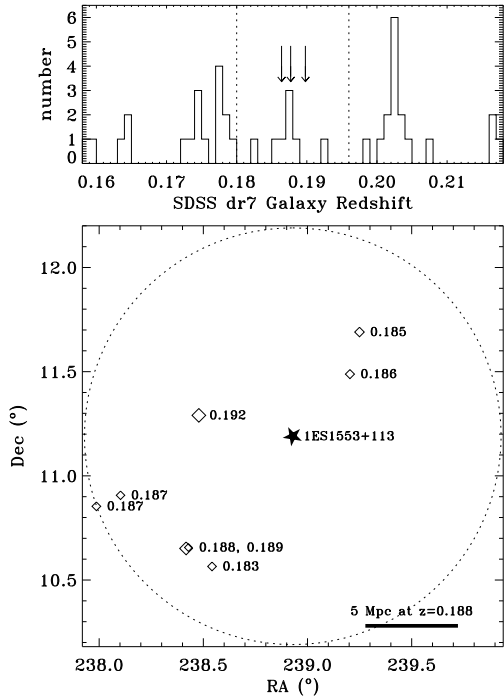


FIG. 6.— Correlating the triple absorption system at $z \sim 0.188$ with SDSS galaxies within one-degree of 1ES 1553+113. The top panel shows a the redshift distribution of SDSS galaxies within the search radius. The three $\text{Ly}\alpha$ absorber redshifts (arrows) correspond to a significant peak in the galaxy distribution bounded by the vertical dotted lines ($0.180 < z < 0.196$). We plot these eight galaxies (diamonds) in relation to the 1ES 1553+113 sight line (star) in the lower panel. Spectroscopic redshifts are noted next to each diamond, and symbol size denotes galaxy luminosity. The distribution of bright galaxies at approximately the redshift of the triple absorption system ($z \sim 0.188$) suggests a large-scale filament. Though none of the SDSS galaxies are closer than $24'$ (~ 4.5 Mpc at $z = 0.188$) to the line of sight, the SDSS galaxy catalog is not complete to lower-luminosity objects at this redshift. All galaxies in this field have $L \gtrsim 3L^*$. A deep galaxy redshift survey will likely show fainter galaxies closer to the AGN line of sight.

skewed toward low-mass stars.

Comparing H I or C III to high ions O VI and N V requires them to be in the same thermal phase for a meaningful analysis. Hybrid ionization modeling (CIE plus photoionization) of the high ions in this system are reported by Yao et al. (2010), in which the $z = 0.1877$ system is used as a test case for a physical parameter-based absorption line modeling exercise.

4.2. Constraining the Redshift of 1ES 1553+113

The redshift of 1ES 1553+113 is crucial to determining the intrinsic properties of the source. Indirect methods of constraining the redshift of 1ES 1553+113 fall into two categories. First, the ratio of AGN to host galaxy optical luminosity in BLLacs is thought to cover a fairly small range (Wurtz, Stocke & Yee 1996; Sbarufatti, Treves, & Falomo 2005). Various deep ground-based (Hutchings & Neff 1992; Scarpa et al. 2000) and space-based (Urry et al. 2000; Carangelo et al. 2003; Sbarufatti et al. 2006; Treves, Falomo, & Uslenghi 2007) optical studies have failed to detect a host galaxy beneath the glare of the AGN. From these non-detections, redshift lim-

its from $z > 0.09$ to $z > 0.78$ have been set by various groups. Treves, Falomo, & Uslenghi (2007) refined this to $z = 0.3 - 0.4$ using a more sophisticated analysis of the same optical data. However, the validity of the assumption of host/nuclear luminosity relationship has been called into question by O'Dowd & Urry (2005).

A complementary technique uses the observed very high energy (VHE) spectrum ($0.1 - 10^3$ GeV) to place limits on the redshift of BL Lacs. This method assumes that the VHE spectral energy distribution (SED) of an object will be modified, as TeV photons interact with photons in the ambient extragalactic background and produce e^+e^- pairs (e.g., Younger & Hopkins 2010; Persic & De Angelis 2008). The longer the pathlength, the steeper the VHE SED becomes. Uncertainties in the extragalactic IR background and the intrinsic SED of the AGN render this method uncertain, but the redshift of 1ES 1553+113 has variously been constrained to $z < 0.74$ (Aharonian et al. 2006; Albert et al. 2007) or $z < 0.80$ or $z < 0.42$ (Mazin & Goebel 2007) based on HESS and MAGIC observations. Abdo et al. (2010) use data from the first six months of *Fermi* γ -ray observations in conjunction with observations from radio wavelengths to 1 TeV to model the intrinsic SED of 1ES 1553+113. Based on these models, they determine a redshift $z = 0.75^{+0.04}_{-0.05}$. The error bars on this estimate appear to be much smaller than justified by this method.

From Figures 1 and 2, it is clear that there are H I systems throughout the redshift range from $z \sim 0$ to near the end of the COS spectral coverage ($z = 0.47$). A strong line at 1695 \AA is identified as $\text{Ly}\alpha$ at $z = 0.395$ and confirmed by detection of O VI at the same redshift in both lines of the doublet. This sets a firm lower limit on $z_{\text{em}} > 0.395$. Two weaker features at 1709.5 \AA and 1741.5 \AA appear in the data, which we identify as $\text{Ly}\alpha$ at $z = 0.4063$ and $z = 0.4326$, respectively. Though we do not detect higher-order Lyman or metal-ion lines at these redshifts, the two $z > 0.4$ $\text{Ly}\alpha$ absorbers are weak enough that we do not expect confirmation in other lines. The continuum of the BL Lac object remains smooth across the entire COS band (Figs. 1 and 2), and no intrinsic emission or absorption is seen.

Thus, we can confidently constrain the emission redshift of 1ES 1553+113 to $z_{\text{em}} > 0.400$, and it appears likely that it may be as high as $z_{\text{em}} = 0.433$. Additional COS observations may detect corresponding $\text{Ly}\beta$ absorption to these two $z > 0.4$ absorbers ($W_{\text{Ly}\beta} \sim 12 \text{ m\AA}$ is expected). The confirmed and unconfirmed direct redshift limits from the HST/COS observations are compatible with both the lower limits set by the non-detection of an optical host galaxy ($z_{\text{em}} \gtrsim 0.1 - 0.4$; Urry et al. 2000; Sbarufatti et al. 2006; Treves, Falomo, & Uslenghi 2007) and the VHE SED upper limits upper limits ($z_{\text{em}} \lesssim 0.8$; Aharonian et al. 2006; Albert et al. 2007; Mazin & Goebel 2007).

We now assess the validity of the most recent VHE SED redshift estimate ($z_{\text{em}} = 0.75^{+0.04}_{-0.05}$) from Abdo et al. (2010). Our current COS far-UV spectra (G130M and G160M) are only sensitive to $\text{Ly}\alpha$ absorbers at $z < 0.47$. However, higher redshift absorbers can be detected using the less sensitive higher-order Lyman lines or O VI doublet. COS far-UV data cover the wavelength range $1135 \text{ \AA} < \lambda < 1795 \text{ \AA}$ corresponding to $\text{Ly}\beta$ redshifts

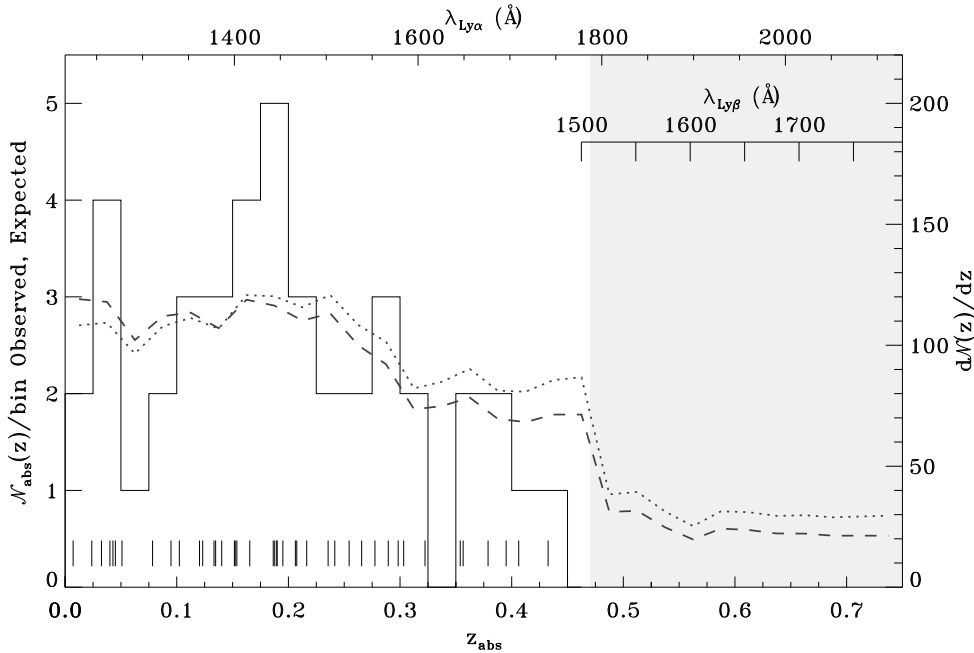


FIG. 7.— Observed and expected distribution of IGM absorbers along the 1ES 1553+113 sight line. Vertical ticks mark the redshift of observed IGM absorbers along the sight line, and the solid line shows a histogram of \mathcal{N}_{abs} per $\Delta z = 0.025$ redshift bin. We calculate the 10σ minimum equivalent width at each redshift bin based on the observed S/N of the data and plot the expected $d\mathcal{N}/dz$ to that limit (dashed curve) based on the large Ly α sample of DS08. If a modest H I absorber evolution is assumed, $d\mathcal{N}_{\text{HI}}/dz \propto (1+z)^{0.7}$, the expected number of IGM systems rises by $\sim 20 - 50\%$ at higher redshifts (dotted curve). At $z > 0.47$ (shaded region), Ly α absorbers can no longer be detected in the COS far-UV band and we must rely on much less sensitive Ly β detections. As discussed in the text, no $z > 0.4$ Ly β absorbers are detected.

$0.11 < z < 0.75$ and O VI redshifts $0.10 < z < 0.74$. Ly β and O VI systems at $z > 0.47$ will appear at $\lambda \gtrsim 1508 \text{ \AA}$. We find empirically (DS08) that the detection threshold for absorption lines with no prior “signposts” (such as known absorber redshifts) is $\sim 10\sigma$. The COS/G160M data in this region are of sufficiently high quality that we would expect to detect lines of $W_{\text{obs}} \gtrsim 50 \text{ m\AA}$ at a $\sim 10\sigma$ significance level. This corresponds to rest-frame $W_r \gtrsim 30 \text{ m\AA}$ for Ly β absorbers at $z \sim 0.5$ or $\log N_{\text{HI}} \gtrsim 13.6$ for Ly β .

Figure 7 shows the observed and predicted distribution of IGM absorbers as a function of redshift. We calculate the expected number of absorbers \mathcal{N}_{abs} per $\Delta z = 0.025$ bin (alternately, $d\mathcal{N}/dz$) based on the S/N-determined minimum equivalent width in each bin and the sample of ~ 650 H I absorbers from DS08. The dashed curve in the figure represents no $d\mathcal{N}/dz$ evolution with redshift. The evolution of low- z H I absorbers is somewhat uncertain. However, if we assume that the H I absorber frequency evolves as $(d\mathcal{N}/dz)_{\text{HI}} \propto (1+z)^\gamma$ (Penton, Stocke, & Shull 2004) and adopt $\gamma \sim 0.7$ for a modest evolution between $z = 0$ and $z \sim 1$, the expected number of H I detections (dotted curve in Figure 7) rises at higher redshift by $\sim 20 - 50\%$. The sharp drop in expected detections at $z > 0.47$ coincides with the switch from Ly α to Ly β as an IGM tracer (shaded area) and the resulting loss of sensitivity discussed above. Summing the expected number of Ly β absorbers ($\mathcal{N}_{\text{abs,exp}}$) which should appear at $\lambda > 1508 \text{ \AA}$ data from Figure 7 over the range $0.47 < z_{\text{abs}} < 0.75$, we find $\mathcal{N}_{\text{abs,exp}} \sim 7$ and $\mathcal{N}_{\text{abs,exp}} \sim 9$ in the constant and evolved H I models, respectively.

Thus, we should expect ~ 8 high- z Ly β absorbers in the 1ES 1553+113 data if $z_{\text{em}} \geq 0.75$.

Are the predicted high- z Ly β absorbers seen? As discussed in §3, the strong feature at 1645.9 \AA can be ruled out as Ly β at $z = 0.6046$ since the corresponding Ly γ line is consistent with Galactic C I (Fig. 4). Thirteen other absorption features longward of 1507 \AA have been identified as Ly α lines, and eight of these identifications are not confirmed with higher-order Lyman or metal-ion lines. If these eight single-line detections are instead interpreted as potential high- z Ly β systems, six have inconsistent Ly γ non-detections and a seventh has Ly γ blended with another line. The only possible high- z Ly β absorber is a marginal line detected at 1584.3 \AA and identified as Ly α at $z = 0.30328$. If this line is instead identified as Ly β at $z = 0.54463$, the corresponding Ly γ absorber should be at 1502.2 \AA , nearly coincident with a weak feature identified as Ly α at $z = 0.23559$. The relative strengths of the two features are consistent with H I absorbers at $z = 0.54463$, but both line detections are of relatively low significance. Additional COS observations may improve the significance of the line detections. However, we find none of the other predicted high- z H I or O VI absorbers in the data, so the $z_{\text{em}} > 0.545$ redshift limit from the possible Ly β detection for 1ES 1553+113 is very speculative.

The additional far-UV observations of 1ES 1553+113 scheduled for HST Cycle 18 will improve the S/N of the current dataset by a factor of ~ 1.7 and consequently lower the minimum detectable line strength for potential Ly β absorbers at $z > 0.47$ by a similar fac-

tor. However, observations with the COS/G185M grating covering the wavelength range $1800 \text{ \AA} \lesssim \lambda \lesssim 2100 \text{ \AA}$ ($0.47 \lesssim z_{\text{abs}} \lesssim 0.73$ in Ly α) would be more efficient at detecting $z > 0.47$ IGM absorbers in the sight line. Despite the relatively lower efficiency of the COS near-UV gratings and detectors compared with their far-UV counterparts, the Ly α lines will be $\sim 3-7$ times stronger than Ly β and should be easily detected or ruled out with only a few kiloseconds of observations. Such observations could potentially also measure weak intrinsic broad-line Ly α emission from the BL Lac object, as has been seen in other BL Lac objects at lower redshift (Danforth, Stocke, Winter, et al., in prep).

We constrain the source redshift of 1ES 1553+113 statistically by truncating the $\mathcal{N}_{\text{abs,expected}}$ model curves in Figure 7 at a range of $0.4 < z_{\text{em}} < 0.75$. Applying a Kolmogorov-Smirnov test to the different models, we set a 1σ constraint of $z_{\text{em}} \leq 0.58$ for the non-evolved model (and $z_{\text{em}} \lesssim 0.49$ for the evolved H I distribution). An emission redshift of ~ 0.75 is ruled out for both models at a 90% or greater level of confidence. Thus, we constrain the redshift of 1ES 1553+113 to the range $0.43 < z_{\text{em}} \lesssim 0.58$.

5. CONCLUSIONS

The BL Lac object 1ES 1553+113 is one of the brightest objects in the sky in γ -rays, as well as being a notable UV and X-ray source. However, the AGN emission is that of a relativistic jet aligned closely with our line of sight and, like most such objects, has no intrinsic emission or absorption features at any wavelength. This featureless, power-law continuum is ideal for measuring intervening IGM features that are weak and broad, such as thermally-broadened Ly α systems. However, the lack of intrinsic features makes constraining the redshift of the object difficult.

We present unprecedented high-quality far-UV HST/COS and *FUSE* spectra of the BL Lac object 1ES 1553+113 at spectral resolution $15-20 \text{ km s}^{-1}$. These data show 42 intervening IGM absorbers, 41 of which are detected in Ly α , and 15 in Ly β and/or metal lines. The richest absorption system in the line of sight is a trio of Ly α absorbers at $z \approx 0.188$ covering $\sim 1000 \text{ km s}^{-1}$ of velocity space. Several metal ions are also detected in these systems, including O VI, N V, and C III. However, neither Si IV nor Si III is detected in any of the systems. The C III/Si III ratio implies a (C/Si) abundance at least four times the solar value, while a high N V/O VI value suggests an overabundance of N as well. A detailed analysis of the physical conditions in this system can be found in Yao et al. (2010).

The redshift of 1ES 1553+113 has never been determined directly, and the only limits placed on it come from indirect means such as the shape of the γ -ray spectrum and the lack of an AGN host galaxy in deep optical images. A strong Ly α +O VI absorber at $z = 0.3951$ gives the first direct lower limit to the redshift of the object. Two weaker Ly α absorbers at $z = 0.4063$ and $z = 0.4326$ give slightly higher estimates of the redshift, but these weak Ly α lines are not confirmed by additional line detections.

These lower limits are consistent with most previous measurements via optical non-detections of host galax-

ies and γ -ray SED constraints. Abdo et al. (2010) derive $z_{\text{em}} = 0.75_{-0.05}^{+0.04}$ based on the latest *Fermi* and TeV γ -ray SED measurements, considerably higher than our intervening absorber upper limits. COS far-UV spectra are not sensitive to Ly α absorbers at $z > 0.47$, but the G160M grating has some sensitivity to intervening Ly β and O VI absorbers out to $z \sim 0.75$. If the Abdo et al. (2010) redshift estimate were accurate, we would expect to find ~ 8 Ly β absorbers at $0.47 < z < 0.75$. We find no evidence for any higher redshift absorption systems. There are only a few absorption features at $\lambda > 1500 \text{ \AA}$ with ambiguous line identifications that could potentially be Ly β systems at $z > 0.47$. While these systems are individually suggestive, we find nowhere near the number of absorbers predicted statistically. We conclude that the redshift of 1ES 1553+113 is not much higher than $z \approx 0.45$.

1ES 1553+113 is one of the brightest X-ray sources on the sky and has been suggested as a sight line that could be efficiently probed for WHIM absorption in O VII. The combined O VI column density in the three absorbers at $z \sim 0.19$ is $\sim 2 \times 10^{14} \text{ cm}^{-2}$. Spectrographs on modern X-ray observatories are sensitive to $\log N_{\text{OVII}} \gtrsim 15.5$. If the temperature of any of these O VI systems is high enough, sufficiently long Chandra and/or XMM/Newton observations may reveal a O VII counterpart to these O VI absorbers that could constrain the long-sought X-ray WHIM (Bregman 2007). However, at the observed Li-like (O VI) oxygen column density, $\log N_{\text{OVI}} \approx 14.3$ in the trio of absorbers, the expected column densities of He-like (O VII) and H-like (O VIII) oxygen are probably just below the detectability levels of *Chandra* and *XMM*. Recent analysis of stacked X-ray absorption data (Yao et al. 2009) at the known IGM redshifts of O VI absorbers finds no evidence for O VII or O VIII absorbers to a limit $N_{\text{OVII}}/N_{\text{OVI}} < 10$. Therefore, the $z \approx 0.19$ absorbers might have X-ray column densities $\log N_{\text{OVII}} \leq 15.3$, just below the limits of current X-ray observatories.

Finally, these observations showcase the powerful new tool available to astronomers for probing the low-redshift IGM. COS is 10 – 20 times more sensitive in the far-UV to point sources than previous instruments on HST. An additional six orbits of COS observations are planned for 2010, which should improve the S/N of the combined dataset by a factor of $\sim \sqrt{3}$. Improving the data quality will help confirm or refute some of the tentative line identifications from this paper and will undoubtedly uncover additional weak absorbers. We will place further constraints on [C/Si] and [N/O] in the $z = 0.188$ system, identify new broad, shallow Ly α absorbers, and investigate possible high- z Ly β systems with our new Cycle 18 observations.

It is our pleasure to acknowledge the many thousands of people who made the HST Servicing Mission 4 the huge success that it was. We furthermore thank Steve Penton, Stéphane Béland, and the other members of the COS ERO and GTO teams for their work on initial data calibration and verification. C. D. wishes to acknowledge a fruitful discussion with members of the KIPAC consortium. This work was supported by NASA grants NNX08AC146 and NAS5-98043 to the University of Colorado at Boulder.

REFERENCES

- Abazajian, K. N., et al. 2009, ApJS, 182, 543
 Abdo, A. A., et al. 2010, ApJ, 708, 1310
 Aharonian, F., et al. 2006, A&A, 448, L19
 Albert, J., et al. 2007, ApJ, 654, L119
 Alber, J., et al. 2009, A&A, 493, 467
 Aleksić, J., et al. 2009, A&A, submitted (ArXiv:0911.1088)
 Asplund, M., Grevesse, N., Sauval, A. J., & Scott, P. 2009, ARA&A, 47, 481
 Bregman, J. N. 2007, ARA&A, 45, 221
 Carangelo, N., Falomo, R., Kotilainen, J., Treves, A. & Ulrich, M.-H. 2003, A&A, 412, 651
 Cayrel, R., et al. 2004, A&A, 416, 1117
 Costamante, L. & Ghisellini, G. 2002, A&A, 384, 56
 Davé, R., et al. 2001, ApJ, 552, 473
 Danforth, C. W., & Shull, J. M. 2005, ApJ, 624, 555
 Danforth, C. W., Shull, J. M., Rosenberg, J. L., & Stocke, J. T. 2006, ApJ, 640, 205 (Paper 2)
 Danforth, C. W., & Shull, J. M. 2008, ApJ, 679, 194 (DS08)
 Danforth, C. W. 2009, in AIP Conf. Proc., *Future Directions in Ultraviolet Spectroscopy*, 1135, eds. G. Sonneborn, M. E. van Steenberg, H. W. Moos, & W. P. Blair, 8
 Danforth, C. W., Stocke, J. T., & Shull, J. M. 2010, ApJ, 710, 613
 Falomo, R. & Treves, A. 1990, PASP, 102, 1120
 Fang, T., Marshall, H. L., Lee, J. C., Davis, D. S., & Canizares, C. R. 2002, ApJ, 572, L127
 Fang, T., Canizares, C. R., & Yao, Y. 2007, ApJ, 670, 992
 Fox, A., Savage, B. D., & Wakker, B. P. 2006, ApJS, 165, 229
 Ghisellini, G., Maraschi, L., & Treves, A. 1985, A&A, 146, 204
 Green, J., et al. 2010, ApJ, in prep.
 Hutchings, J. B., & Neff, S. G. 1992, AJ, 104, 1
 Lehner, N., Savage, B. D., Richter, P., Sembach, K. R., Tripp, T. M., & Wakker, B. P. 2007, ApJ, 653, 680
 Mazin, D. & Goebel, F. 2007, ApJ, 655, L13
 McWilliam, A. 1997, ARA&A, 35, 503
 Meisner, A. M., & Romani, R. W. 2010, ApJ, submitted (ArXiv:1002.1343)
 Miller, H. R., & Green, R. F. 1983, BAAS, 15, 957
 Moos, H. W., et al. 2000, ApJ, 538, L1
 O'Dowd, M., & Urry, C. M. 2005, ApJ, 627, 97
 Osterman, S., et al. 2010, ApJ, in prep
 Penton, S. V., Stocke, J. T., & Shull, J. M. 2004, ApJS, 152, 29
 Persic, M. & De Angelis, A. 2008, A&A, 483, 1
 Richter, P., Savage, B. D., Tripp, T. M., & Sembach, K. R. 2004, ApJS, 153, 165
 Sahnou, D. J., et al. 2000, ApJ, 538, L7
 Savage, B. D., et al. 2010, in prep.
 Sbarufatti, B., Treves, A., Falomo, R. 2005, ApJ, 635, 173
 Sbarufatti, B., Treves, A., Falomo, R., Heidt, J., Kotilainen, J. & Scarpa, R. 2006, AJ, 132, 1
 Scarpa, R., Urry, C. M., Falomo, R., Pesce, J.E., & Treves, A. 2000, ApJ, 532, 740
 Shull, J. M., Jones, J. R., Danforth, C. W., & Collins, J. A. 2009, ApJ, 699, 754
 Treves, A., Falomo, R., & Uslenghi, M. 2007, A&A, 473, L17
 Urry, C. M., Scarpa, R., O'Dowd, M., Falomo, R., Pesce, J. E. & Treves, A. 2000, ApJ, 532, 816
 Woosley, S. E., & Weaver, T. A. 1995, ApJS, 101, 181
 Wurtz, R., Stocke, J. T., Yee, H. K. C. 1996, ApJS, 103, 109
 Yao, Y., Tripp, T. M., Wang, Q. D., Danforth, C. W., Canizares, C. R., Shull, J. M., Marshall, H. L., & Song, L. 2009, ApJ, 697, 1784
 Yao, Y., et al. 2010, in prep.
 Younger, J. D., & Hopkins P. F. 2010, MNRAS, submitted (arXiv:1003.4733)

TABLE 1
 INTERGALACTIC LINE DETECTIONS

z_{abs}	Line	W_r (mÅ)	b (km s $^{-1}$)	log N	notes
0.00717	Ly α	108 \pm 12	35 \pm 4	13.37 \pm 0.04	blend with O VI $z = 0.187$
0.02386	Ly α	54 \pm 8	19 \pm 4	13.07 \pm 0.05	
0.03254	Ly α	24 \pm 8	13 \pm 7	12.70 \pm 0.10	weak
0.04012	Ly α	215 \pm 9	27 \pm 1	13.86 \pm 0.02	
	Ly β^a	87 \pm 46	11 \pm 6	14.39 \pm 0.22	ambiguous ID
			17 $^{+21}_{-5}$	14.25 $^{+0.78}_{-0.47}$	HI COG solution b
0.04281	Ly α	135 \pm 14	73 \pm 7	13.44 \pm 0.04	broad
0.04498	Ly α	275 \pm 10	47 \pm 2	13.87 \pm 0.01	asymmetric
	Ly β^a	90 \pm 8	45 \pm 2	14.19 $^{+0.09}_{-0.09}$	
			24 $^{+3}_{-3}$	14.20 \pm 0.07	HI COG solution b
0.05094	Ly α	84 \pm 9	17 \pm 3	13.32 \pm 0.04	
0.07832	Ly α	58 \pm 10	24 \pm 6	13.09 \pm 0.06	weak
0.09481	Ly α	176 \pm 9	30 \pm 2	13.67 \pm 0.02	
	Ly β^a	34 \pm 8	26 \pm 11	13.80 $^{+0.17}_{-0.19}$	weak, ambiguous ID
			28 $^{+\infty}_{-10}$	13.70 $^{+0.13}_{-0.14}$	HI COG solution b
0.10230	Ly α	360 \pm 4	52 \pm 1	14.12 $^{+0.03}_{-0.03}$	BLA?
	Ly β^a	81 \pm 10	36 \pm 12	14.20 $^{+0.12}_{-0.11}$	
			42 $^{+12}_{-6}$	14.10 \pm 0.08	HI COG solution b
0.12040	Ly α	32 \pm 7	21 \pm 9	12.85 $^{+0.07}_{-0.14}$	weak
0.12325	Ly α	77 \pm 17	81 \pm 16	13.18 \pm 0.07	weak, broad
	Si III 1206	16 \pm 8	9 \pm 8	11.93 \pm 0.14	tentative
0.13334	Ly α	70 \pm 13	46 \pm 8	13.15 \pm 0.06	
0.13483	Ly α	156 \pm 9	30 \pm 2	13.60 \pm 0.02	
0.14028	Ly α	28 \pm 8	18 \pm 8	12.76 \pm 0.10	weak
0.15164	Ly α	51 \pm 9	28 \pm 6	13.02 \pm 0.06	
0.15234	Ly α	173 \pm 13	66 \pm 5	13.56 \pm 0.03	
0.15380	O VI 1038	50 \pm 9	26 \pm 6	13.95 \pm 0.06	tentative, see §3, Fig. 3
0.16540	Ly α	35 \pm 8	40 \pm 11	12.83 \pm 0.09	weak

TABLE 1
INTERGALACTIC LINE DETECTIONS

0.18640	$\text{Ly}\alpha$	139 ± 7	32 ± 2	13.52 ± 0.02	
	$\text{Ly}\gamma$	10 ± 7	~ 5	13.84 ± 0.56	weak
0.18773			$17_{-6}^{+\infty}$	$13.67_{-0.24}^{+0.27}$	poorly-constrained HI COG ^b
	O VI 1038	10 ± 4	~ 5	13.40 ± 0.24	low significance
	C III 977	26 ± 11	22 ± 14	12.64 ± 0.15	noisy
	$\text{Ly}\alpha$	293 ± 8	50 ± 1	13.89 ± 0.01	double
0.18958	$\text{Ly}\gamma$	23 ± 32	15 ± 12	14.02 ± 0.27	marginal
			$36_{-14}^{+\infty}$	$13.99_{-0.18}^{+0.44}$	poorly-constrained HI COG ^b
	O VI 1032	108 ± 16	41 ± 6	$14.04_{-0.06}^{+0.08}$	complicated structure
	O VI 1038	68 ± 2	35 ± 1	$14.11_{-0.04}^{+0.04}$	
	N V 1238	74 ± 7	36 ± 4	$13.62_{-0.04}^{+0.07}$	two components
	N V 1242	50 ± 11	36 ± 9	13.71 ± 0.08	single component
	C III 977	89 ± 6	36 ± 5	$13.25_{-0.04}^{+0.06}$	two components
	Si II 1260	~ 18	~ 5	12.1 ± 0.2	two components, tentative
	$\text{Ly}\alpha$	85 ± 17	49 ± 13	13.24 ± 0.11	
	0.18989	$\text{Ly}\alpha$	74 ± 8	28 ± 4	13.20 ± 0.05
$\text{Ly}\gamma$		21 ± 10	7 ± 10	14.03 ± 0.15	weak
O VI 1032		38 ± 8	21 ± 6	13.53 ± 0.07	
O VI 1038		16 ± 5	13 ± 9	$13.48_{-0.19}^{+0.14}$	
0.19503	$\text{Ly}\alpha$	124 ± 7	32 ± 2	13.45 ± 0.02	
0.20621	$\text{Ly}\alpha$	58 ± 12	44 ± 10	13.06 ± 0.07	weak
0.20747	$\text{Ly}\alpha$	53 ± 12	44 ± 11	13.02 ± 0.08	weak
0.21640	$\text{Ly}\alpha$	87 ± 14	46 ± 7	13.25 ± 0.05	
0.23559	$\text{Ly}\alpha$	20 ± 7	12 ± 8	12.62 ± 0.12	weak
0.24155	$\text{Ly}\alpha$	242 ± 10	36 ± 2	13.84 ± 0.02	strong, multi-component?
	$\text{Ly}\beta$	34 ± 5	26 ± 7	$13.73_{-0.10}^{+0.07}$	weak
0.25439	$\text{Ly}\alpha$	68 ± 2	31 ± 2	$13.17_{-0.05}^{+0.04}$	
0.26560	$\text{Ly}\alpha$	46 ± 10	26 ± 7	12.97 ± 0.08	weak
0.27753	$\text{Ly}\alpha$	77 ± 10	26 ± 4	13.22 ± 0.05	
0.28944	$\text{Ly}\alpha$	56 ± 10	24 ± 6	13.07 ± 0.07	
0.29830	$\text{Ly}\alpha$	56 ± 12	19 ± 5	13.09 ± 0.07	
0.30328	$\text{Ly}\alpha$	70 ± 7	34 ± 6	$13.20_{-0.08}^{+0.06}$	weak, noisy
0.32235	$\text{Ly}\alpha$	190 ± 4	34 ± 4	13.73 ± 0.04	
	$\text{Ly}\beta$	55 ± 9	38 ± 7	13.92 ± 0.06	
0.35390			18_{-2}^{+4}	$13.98_{-0.11}^{+0.10}$	HI COG solution ^b
	$\text{Ly}\alpha$	235 ± 21	~ 79	13.73 ± 0.03	tentative, see §3, Fig. 4
0.35650	$\text{Ly}\alpha$	170 ± 14	43 ± 4	13.60 ± 0.03	
	$\text{Ly}\beta$	31 ± 9	28 ± 9	13.66 ± 0.10	
0.37884			$28_{-12}^{+\infty}$	$13.66_{-0.16}^{+0.15}$	poorly-constrained HI COG ^b
	$\text{Ly}\alpha$	136 ± 19	47 ± 6	13.47 ± 0.06	
	$\text{Ly}\beta$	23 ± 5	15 ± 5	13.55 ± 0.08	
0.39505			$27_{-15}^{+\infty}$	13.54 ± 0.12	poorly-constrained HI COG ^b
	$\text{Ly}\alpha$	278 ± 18	57 ± 4	13.84 ± 0.02	multiple components
	$\text{Ly}\beta$	38 ± 1	~ 54	$13.76_{-0.05}^{+0.07}$	broad, multi-component
	O VI 1032	57 ± 6	31 ± 4	13.71 ± 0.04	
0.40630			27 ± 4	$13.69_{-0.08}^{+0.09}$	
	O VI 1038	27 ± 4	23 ± 5	$13.13_{-0.06}^{+0.11}$	weak
0.43261	$\text{Ly}\alpha$	89 ± 6	32 ± 2	$13.31_{-0.05}^{+0.07}$	noisy

^a Measurement based on *FUSE* data.

^b Curve of growth b_{HI} , N_{HI} solution based on multiple Lyman lines.